**COMMUNICATIONS IN SCIENCE AND TECHNOLOGY**
*Homepage:* cst.kipmi.or.id

# Flat mixed matrix membranes incorporating MIL-53(Al) and polyethersulfone for highly selective $H_2/CO_2$ and $H_2/CH_4$ separation

Jeesica Hermayanti Pratama[a,b,c], Burhan Fatkhur Rahman[a,b], Fauziyah Azhari[a,b], Triyanda Gunawan[c], Nurul Widiastuti[c], Hamzah Fansuri[c], Desi Suci Handayani[a], Shinta Amelia Putri[a,b], Witri Wahyu Lestari[a,b*]

[a]*Chemistry Department, Universitas Sebelas Maret, Surakarta 57126, Indonesia*
[b]*Research Group Porous Materials for Sustainability, Surakarta 57126, Indonesia*
[c]*Department of Chemistry, Institut Teknologi Sepuluh Nopember, Surabaya 60111, Indonesia*

*Article history:*
Received: 31 March 2026 / Received in revised form: 20 June 2026 / Accepted: 20 June 2026

**Abstract**

The integration of metal-organic frameworks (MOFs) as fillers in hybrid membranes commonly termed mixed matrix membranes (MMMs) represents a significant advancement in the field of gas separation technology. This present study proposes novel MMMs for the separation of $H_2$, $CH_4$, and $CO_2$. The Material Institute of Lavoisier framework (MIL-53(Al)) was incorporated into a polyethersulfone (PES) matrix at filler loadings of 10%, 20%, and 30% (w/w). IR and SEM analyses confirmed that the irregular MIL-53(Al) particles were uniformly dispersed within the PES matrix. The gas separation performance was evaluated using both single gas feeds ($H_2$, $CO_2$, $CH_4$) and mixed gas feeds ($H_2/CO_2$ and $CO_2/CH_4$) under 2 bar pressure at 30 °C. In comparison to the pristine PES membrane, the incorporation of MIL-53(Al) considerably enhanced gas permeability, with the 30% MIL-53(Al)@PES membrane demonstrating remarkable single-gas permeation performance. It is also notable that the membrane containing 20% MIL-53(Al) achieved the highest selectivity for $H_2/CO_2$ and $CO_2/CH_4$ (3.28), representing a 54.72% improvement over the pristine PES membrane. Interestingly, almost all MIL-53(Al)@PES membranes exhibited exceptional $H_2/CO_2$ separation performance, exceeding the Robeson upper bound. However, for the $H_2/CH_4$ and $CO_2/CH_4$ mixed gas separation tests, the selectivity of 1.82 and 0.32, respectively, was observed for the 20% MIL-53(Al) membrane, closely resembling the performance of the pure PES membrane. The present work demonstrates that the integration of MIL-53(Al) into PES is an effective strategy to enhance membrane penetrability and $H_2/CO_2$ separation performance, thereby highlighting its potential for the improvement of MOF-based mixed matrix membranes for selective gas separation.

*Keywords:* Hydrogen separation; MIL-53(Al); membrane; PES

## 1. Introduction

The increasing reliance on fossil fuels for energy has emerged as a significant contributor to global warming and a myriad of climate-related challenges. The extensive consumption of fossil fuels for energy production has been identified as a key factor in the emission of carbon dioxide ($CO_2$) emissions, which is recognized as a major driver of the long-term greenhouse effect. As revealed by data from the World Meteorological Organization, the earth's average temperature has increased by more than 1 °C since the onset of industrial processes, thereby underscoring an urgency for action to be taken in response to climate change [1]. It is important to note that $CO_2$ accounts for a significant portion of climate forcing, thus highlighting its critical role in exacerbating global warming [2]. The awareness of these impacts has led to a growing consensus that innovative solutions and cleaner energy alternatives are essential for mitigating the adverse effects of fossil fuel consumption and ensuring a sustainable future.

As fossil fuel companies have historically underestimated the environmental consequences of their operations, the transition to renewable energy sources has become increasingly imperative [3]. This transition is of critical importance in addressing the urgent climate crisis, whilst also providing support global initiatives aimed at reducing greenhouse gas emissions and promoting sustainable energy systems [2,4].

It is increasingly recognized that hydrogen ($H_2$) is a pivotal alternative fuel that offers ecological benefits and a cleaner energy profile in comparison with conventional fossil fuels. Its high energy density, estimated at approximately 120-142 kJ/g, positions hydrogen as a promising energy carrier capable of addressing critical challenges associated with climate change

* Corresponding author.
Email: witri@mipa.uns.ac.id
https://doi.org/10.21924/cst.11.1.2026.1954

and persistent air pollution [5,6]. The abundance of hydrogen, in conjunction with its capacity to be produced through methods such as SMR, water electrolysis, and biomass gasification, emphasize its potential as a sustainable energy carrier [7,8,9]. Despite its advantages inherent in the process, there are challenges associated with hydrogen production. The predominant method of hydrogen generation, SMR, results in significant carbon dioxide ($CO_2$) emissions, thus necessitating effective separation processes to purify the hydrogen from byproducts such as $CO_2$ and methane ($CH_4$) [10,11]. Continuous purification during hydrogen production, particularly through water-gas shift (WGS) reactions, is crucial to enhance the overall efficiency and reduce the environmental impact of hydrogen generation [10,12]. Moreover, advancements in membrane technology have demonstrated potential in facilitating continuous separation of hydrogen, thereby overcoming thermodynamic limitations and enhancing carbon conversion rates [9,12].

Numerous methods are available for the purification of hydrogen; among the most commonly employed techniques are pressure swing adsorption (PSA) and cryogenic distillation. However, these methods frequently yield hydrogen with insufficient purity, necessitating additional purification steps that can lead to increased costs and energy consumption [13]. In contrast, membrane-based gas separation technologies offer a more favorable alternative due to their inherent advantages, including lower energy requirements, reduced carbon footprints, operational simplicity, and the potential to achieve higher purity levels of hydrogen [14,15]. The mechanism of solution-diffusion enables membranes to function as selective barriers, thereby effectively separating hydrogen from other gases in a mixture [14,15]. In the context of a comparison of various gas separation techniques for $H_2/CO_2/CH_4$ mixtures, the limitations associated with polymer membranes - specifically the trade-offs concerning permeability and selectivity can be mitigated through the use of mixed matrix membranes (MMMs) [16]. Polyethersulfone (PES) based polymer membranes have gained prominence in separation processes due to their extraordinary mechanical strength, excellent chemical and thermal resistance, and ease of fabrication [17]. Furthermore, the relatively elevated glass transition temperatures of PES membranes may enhance their applicability in separation processes, particularly during water-gas shift reactions, where the maintenance of structural integrity under varying thermal conditions is deemed imperative. Recent advancements in membrane technology, including the development of palladium-based membranes, have further improved the efficiency of hydrogen separation. These membranes have been demonstrated to be highly effective in achieving high purity levels from gas mixtures with low hydrogen concentrations, despite requiring elevated operating temperatures [15]. The integration of these advanced materials into existing hydrogen purification systems has the potential to enhance the efficiency and sustainability of hydrogen production processes to a substantial degree.

The trend of introducing fillers into PES polymers with a view to enhancing the separation performance has been the subject of extensive research, including activated carbon-based materials [18], metal-organic frameworks (MOFs) [19], clay [20], and metal oxide [21]. Among others, MOFs offer numerous advantages, including their ability to exhibit controllable physicochemical properties, for instance tunable pore size, high surface area, and diverse range of functionalities due to their wide range of metal ions and organic linkers types that can be utilized as precursors. The introduction of MOFs as the filler has been demonstrated to produce a favorable interface with the polymeric matrix to enhance gas separation performance in MMMs [22].

Previous studies regarding the addition of MOF fillers into PES polymers have been conducted, including HKUST-1 [23], MIL-96(Al) [24], MIL-100(Al) [25], and ZIF-8 [26]. MIL-53, in particular, has developed as a unique form of crystalline highly porous material as a subfamily of MOFs. It has been evidenced that MIL-53(Al) is the most thermally stable type of MIL-53 family, and it is applicable at temperatures of up to 500 °C. With such characteristic, it is assumed that the employment of MIL-53(Al) as a filler in polymeric membranes has the potential to result in a good physicochemical property. MIL-53(Al) is composed of aluminum as the metal ion core and ligands containing terephthalic groups. These MOFs feature malleable crystalline structures that can vary their pore size in response to temperature, gas adsorption, and the majority of organic solvents. In addition, MIL-53(Al) exhibits a distinctive structural alteration characterized by pore expansion as a result of heat stimulation and pore constriction due to gas adsorption, referred to as the breathing effect [27]. More specifically, with the incorporation of guest molecules such as gas molecules, as well as applied pressure, MIL-53(Al) frameworks undergo an adjustable pore structural shift, modifying the gas separation capability of the MOF in MMMs [28].

Most studies reported that MIL-53(Al) and its post-modification have been widely applied in the separation of $CO_2/N_2$ or $CO_2/CH_4$ [19,28,29,30]. The study by Basu et al. [31] discovered that the incorporation of MIL-53(Al) into Matrimid membranes resulted in enhanced $CO_2/CH_4$ and $CO_2/N_2$ separation enactment. However, only a limited number of research reports have been published thus far on the $H_2/CO_2$ or $H_2/CH_4$ separation performance of MOF-contained MMMs. Adams et al. investigated the loading of MOF-5 into polyethyleneimine (PEI), with the aim of enhancing $H_2$ permeability up to 40% more than pristine PEI membrane [32]. Japip et al. observed that loading ZIF-71 on 6FDA-Durene resulted in an increased separation of $H_2/CH_4$ [33]. A previous study by Ercan et al. [27] informed that the incorporation of 40% MIL-53(Al) in cyclic olefin copolymer (COC) has been shown to increase $H_2$ permeability by up to 59%. In this study, the performance of MIL-53(Al) loaded on PES-based MMMs is further explored to separate hydrogen gas from $CO_2$ and $CH_4$ mixtures ($H_2/CO_2$ and $H_2/CH_4$), which, to the best of our knowledge, has not been reported so far. The presence of narrow and large pores in MIL-53(Al) has been shown to control the gas transportation, thereby enabling selective separation.

## 2. Materials and Methods

### *2.1. Materials*

The following substances were purchased from Merck EMSURE: aluminum nitrate nonahydrate ($Al(NO_3)_3 \cdot 9H_2O$,

98.5%), benzene-1,4-dicarboxylic acid ($H_2BDC$, 98%), N, N'-Dimethylformamide (DMF, 99.8%), methanol (MeOH, 99.9%), polyethersulfone (PES, 99.99%), ethanol (EtOH, ≥99.9%), and N, N'-Dimethyl acetamide (DMAc, ≥99%). The high-purity gases utilized in the permeation tests included carbon dioxide ($CO_2$, 99.9%), methane ($CH_4$, 99.995%), and hydrogen ($H_2$, 99.9%). The performance of binary gas separation was conducted on an equimolar gas pair of hydrogen and methane ($H_2/CH_4$).

### *2.2. Preparation of MIL-53(Al)*

MIL-53(Al) sample was prepared under solvothermal conditions, following a modified technique that has been documented in the literature [34]. $Al(NO_3)_3•9H_2O$ (1 mmol, 0.937 g) and $H_2BDC$ (2.25 mmol, 0.934 g) were dissolved in 25 mL of DMF and stirred for a period of half an hour. The solution was placed into a 50 mL Teflon-lined autoclave and heated at 120 °C for a duration of 24 hours in an oven (Memmert Atmosafe UN30-1060 E7086). The resulting white precipitate was collected (by filtration) after cooling to ambient temperature. This was then washed three times with DMF (25 mL) to remove any remaining ligands. Subsequently, the precipitous was purified once with methanol (25 mL) under stirring for a period of 3 hours. The obtained MIL-53(Al) was then subjected to heating overnight at 100 °C and continued activated at 155 ºC for 24 hours prior to the measurement of the nitrogen sorption isotherm.

### *2.3. Preparation of MMMs*

The fabrication of hybrid membranes was undertaken through the phase inversion method. The PES was dissolved at a concentration of 35% (w/w) in 15 mL DMAc and stirred for 24 hours to generate a homogenous dope solution. The loading variations of MIL-53(Al) on PES were 10, 20, and 30% (w/w). The attained dope solution was then molded on flat glass and immersed in a water coagulant bath until the membrane could be peeled off and withered at room temperature for a period of 24 hours.

### *2.4. Gas permeation test*

The gas permeation capabilities of PES/MIL-53(Al) were assessed by pure and mixed gas measurements in a laboratory-scale module adapted from Gunawan et al. [35] in SI Fig. S1. The permeability of $H_2$, $CO_2$, and $CH_4$ pure gases was measured at room temperature and a pressure of 2 bars. The membranes with a diameter of 5 mm were fixed using a module that was sealed with O-rings in the membrane reactor. The selectivity of the mixed gas was analyzed by means of Shimadzu GC-08. The calculation of permeability was performed using the following Eq. (1).

$$P_x = (Q\ x\ t)/(\Delta P\ x\ A) \quad (1)$$

where Q represents the volumetric gas flow rate at standard condition ($cm^3$ (STP) $s^{-1}$), P refers to the applied pressure (cmHg), l is the selective layer width of the membrane (cm), and A is the membrane effective surface area ($cm^2$). Therefore, the ultimate selectivity of the membranes was considered by dividing the permeability value of the two gases separated, as given in Eq. (2).

$$A(x, y) = Px/\mathrm{Py} \quad (2)$$

where P$x$ and Py are the permeability of gas x and gas y, respectively.

The data acquisition replication was conducted three times for permeability measurement and further three times for mixed gas selectivity. The data and its averages are presented in SI Table S5. The mixed-gas permeation measurement was conducted on 2 equimolar mixtures of $H_2/CH_4$ and $CO_2/CH_4$, with the method adapted from Lin et al. [36] and Gunawan et al. [37].

### *2.5. Material characterization*

X-ray powder diffraction (XRD) was measured utilizing an Expert Pan Analytical diffractometer, with Cu K-α radiation (8.04 keV, x-ray wavelength of 1.5406 Å). The diffraction was collected at 2 thetas in the range of 5 – 50°. The superficial and cross-sectional morphology of MMMs were observed by means of a Zeiss Evo X microscope, while the functional groups present in both MIL-53(Al) and the MMMs were observed using a Shimadzu IR Prestige 21. Thermal stability was assessed between 30 and 900 °C under $N_2$ atmosphere at a heating speed of 10 °C/min using a STA Linseis PT 1600. Additionally, the pore size distribution and external area of the activated MIL-53(Al) were quantitatively analyzed via nitrogen adsorption at 77K using a Quantachrome QuadraSorb instrument.

## 3. Results and Discussion

### *3.1. MIL-53(Al) characterization*

The diffraction peaks obtained from XRD were consistent with pure-phase MIL-53(Al), thus confirming the successful synthesis of the material. As demonstrated in Fig. 1, the synthesized MIL-53(Al) (blue line) exhibited all characteristic peaks, which were well matched with the reference pattern of MIL-53(Al) from CCDC 220475 (red line) at 8.8°, 10.3°, 15.2°, 17.7°, 21.2°, 24.1°, 25.3°, and 26.8°, respectively, corresponding to the (2 0 0), (1 1 0), (1 1 –1), (4 0 0), (1 1 1), (0 2 0), (2 2 0), (0 2 1) of MIL-53(Al) planes as reported in previous literature [38]. In general, prominent peaks and long-range order in the material's diffractogram pattern indicate a high degree of crystalline nature [39] and well-aligned crystallographic structures at the atomic level.

To verify the purity of the prepared MIL-53(Al) and evaluate the existence of residual $H_2BDC$ ligand, the Le Bail refinement method was performed using Rietica software. The result in SI Fig. S2 confirmed that the material was 97.02% molar MIL-53(Al). The low $R_p$ and $R_{wp}$ values, respectively, 6.23% and 8.01%, indicate that a high-reliability index of the diffraction patterns and weight were achieved in this research [24].

Further infrared analysis of the synthesized MIL-53(Al) is presented in SI Fig. S3, confirming that the MIL-53(Al) has

been formed to align with the standard peaks' literature. A significant change of absorption peaks was observed from 2540 and 3102 $cm^{-1}$ to 1509 and 1604 $cm^{-1}$ (asymmetrical stretching) and 1416 and 1440 $cm^{-1}$ (symmetrical stretching). This alteration indicates the deprotonation of the carboxylic acid group in $H_2BDC$ ligand and coordinated to $Al^{3+}$ ion from the metal salt precursor. Thus, the vibration observed at 3680 $cm^{-1}$ is consistent with the bending mode of $AlO_4(OH)_2$ or $\mu_2$-hydroxo-bridging group on the Al(III). The absorption bands at 3402 $cm^{-1}$ are associated to the stretching vibration of water molecules coordinated on the MIL-53(Al). These results align with the findings of a previous study [40].

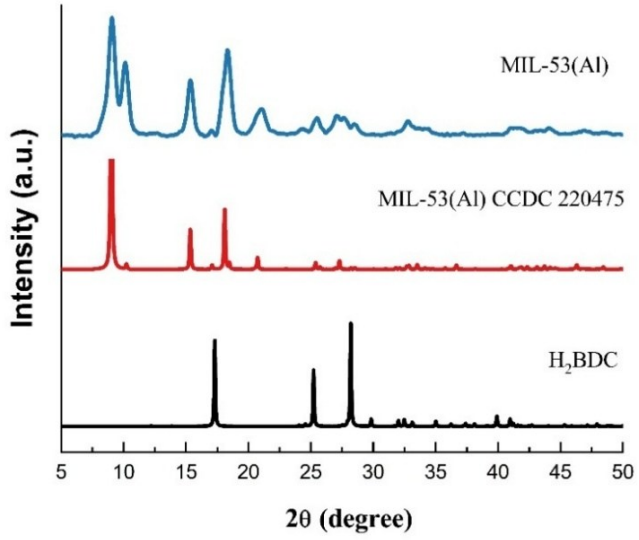


Fig. 1. X-Ray diffractogram of synthesized MIL-53(Al), CCDC standard, and precursor ligand

SI Fig. S4 illustrates the distribution of particles and their morphology as observed through the SEM analysis of synthesized MIL-53(Al). The result demonstrates an irregular shape aggregation of the prepared MIL-53(Al) with a typical particle size diameter of approximately 120 nm. The results of this study indicate that particle size is smaller than the result conducted by Chakraborty and Acharya [38], with an average length of MIL-53(Al) between 200–300 nm. The heating applied in the solvothermal synthesis produced a higher solubility of reactants.

The thermal investigation of MIL-53(Al) reveals two stages of mass loss profile, as depicted in SI Fig. S5. The first mass loss of the MIL-53(Al) framework was observed to occur at temperature below 100 °C and was attributed to the loss of hydroxyl molecule. The second mass loss at temperature above 500 °C is attributable to the decomposition of the MOF framework, with the loss of BDC ligand molecule. In the present study, the 59.97% mass loss of synthesized MIL-53(Al) was found to be align to the findings of previous study [38], which reported a loss of approximately 50%, indicating that the solvothermal method also produced good thermal stability of MIL-53(Al).

### *3.2. Characterization of MMMs*

The characterization of MMMs was carried out through FTIR, TGA, and SEM investigation to determine the effect of MIL-53(Al) addition to PES polymer. As illustrated in Fig. 2, the FTIR spectra of MIL-53(Al) and MIL-53(Al)@PES at different loading variations were compared. MIL-53(Al) fillers demonstrated no chemical interaction with PES as the polymer matrix. A number of characteristics of PES absorption were identified in MIL-53(Al)@PES. The stretching vibration of symmetrical and asymmetrical O=S=O was observed at ~1325 and ~1151 $cm^{-1}$, respectively; C–H and C=C stretching of the aromatic ring appeared at ~2939 and ~1506 $cm^{-1}$, respectively; and C–O–C stretching of ether was identified at ~1104 $cm^{-1}$. The incorporation of MIL-53(Al) as filler particles with higher percentage loadings exhibits an influence on the characteristic peak visibility in MMMs. The O–H from MIL-53(Al) showed a peak at approximately 3440 $cm^{-1}$, while the stretching of C=O asymmetrical was observed at around 1610 $cm^{-1}$. The presence of C–H can be observed at around 700–1100 $cm^{-1}$. Furthermore, the Al–O bond from MIL-53(Al) was found at approximately 485 $cm^{-1}$ in MMMs. As depicted in Fig. 2, no new peak was identified. All absorption peaks at several ranges are consistent with the previous research [18,41].

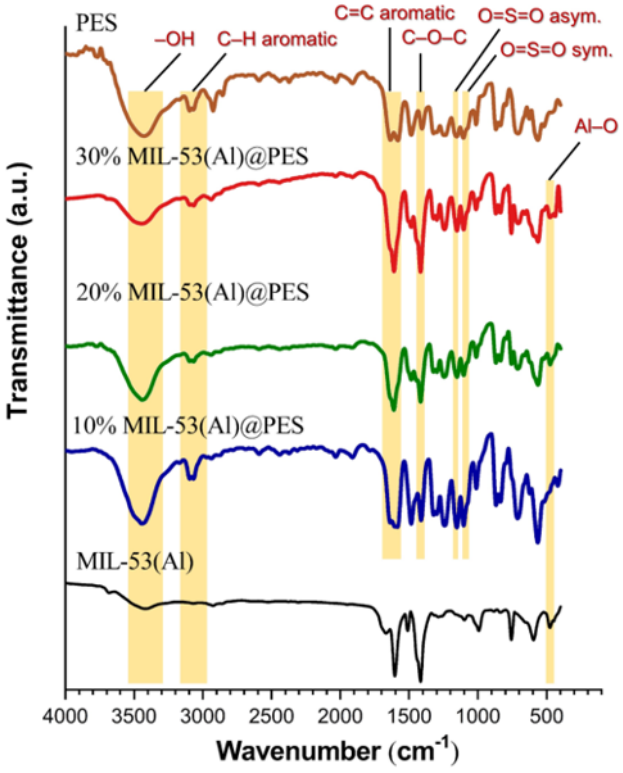


Fig. 2. FTIR spectra of pristine MIL-53(Al), neat PES, and MIL-53(Al)@PES with various of loading

As presented in Fig. 3, the XRD pattern of pristine PES displays a broad amorphous halo centered at 2θ ≈ 17.9°, corresponding to an average d-spacing of approximately 4.96 Å. This confirms the non-crystalline nature of the polymer matrix [42,43]. The diffractogram of MIL-53(Al) displays sharp reflections at low angles (around 9–10° and 15–18°), in agreement with the reference pattern reported earlier, indicating a well-crystallized MOF phase [44]. Upon incorporation of MIL-53(Al), the MMMs retain this broad feature yet additional low-angle reflections characteristic of MIL-53(Al) becomes clearly visible. This is particularly evident for the 20 and 30 wt.% loadings, where pronounced peaks appear around 2θ ≈ 9.1–9.3° and 10.0–10.3°. These

reflections correspond to d-spacings of approximately 9.7 and 8.6 Å, respectively, and are consistent with the low-angle MIL-53(Al) peaks reported in Section 3.1 and in the reference pattern from CCDC 220475. For the 10 wt.% MIL-53(Al)/PES membrane, the diffractogram is dominated by the PES amorphous halo, with a representative maximum at $2\theta \approx 18.3°$ ($d \approx 4.85$ Å). This suggests that the polymer matrix remains the main scattering phase and that the MIL-53(Al) reflections are partially masked by the background [45]. In contrast, the 20 and 30 wt.% MMMs exhibit a clear coexistence of the MIL-53(Al) low-angle peaks at approximately 9–10° and the broad PES feature at approximately 18.4–18.6°, with calculated d-spacings of 9.47–9.71 Å and 4.76–4.84 Å, respectively. This finding confirms that the MIL-53(Al) particles maintain their crystalline framework following phase inversion and casting into the PES matrix, in line with the SEM observations of uniformly dispersed filler domains within the membrane structure [46]. The slight shift of the amorphous PES halo from 4.96 Å in the pristine membrane to 4.85–4.76–4.83 Å in the 10, 20, and 30 wt.% MMMs is modest and should not be over-interpreted as evidence for strong chemical interactions or a polymer phase transition. Instead, this change is more plausibly explained by local perturbations of chain packing and free-volume distribution induced by the dispersed MIL-53(Al) domains. This is a reliable explanation, as evidenced by the FTIR spectra that show no new absorption bands upon MOF addition. The coexistence of an amorphous PES matrix and crystalline MIL-53(Al) domains has been demonstrated to be compatible with the gas-transport behavior discussed in Section 3.3. In this regard, the MOF phase has been shown to enhance permeability while the polymer matrix continues to control membrane integrity and part of the selectivity trade-off.

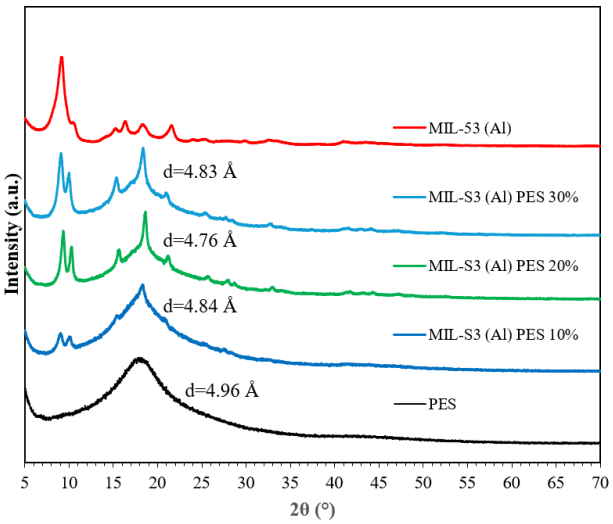


Fig. 3. X-ray diffractograms of MMMs containing different MIL-53(Al) loadings, compared with synthesized MIL-53(Al) and neat PES

As depicted in Fig. 4, the differences in thermal characteristics of MMMs with the incorporation of different MIL-53(Al) are evident. The first mass loss at approximately 200 °C indicated the evaporation of DMAc solvent utilized in the dope solution of the membranes. At the temperatures above 450 °C, the decomposition of PES begins [18], which clearly also occurred in MMMs. Generally, the addition of MIL-53(Al) at 10, 20, and 30% (w/w) does not significantly change the thermal stability of the MMMs. Nevertheless, the findings of this study demonstrate the potential application of the fabricated membranes at high temperatures (up to approximately 400 °C) before the decomposition may reduce its performance. This membrane's high thermal stability supports the application in the hydrogen separation from water-gas shift reaction occurred at high temperature.

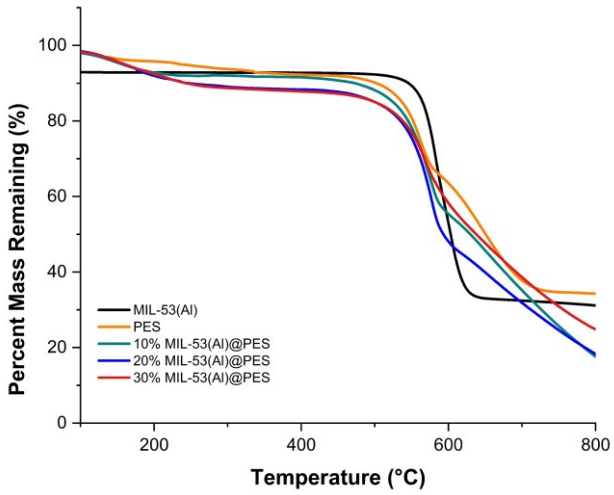


Fig. 4. TGA curves of MMMs with different loadings of MIL-53(Al)

Fig. 5 and Fig. 6 illustrate the morphology of asymmetrical MMMs MIL-53(Al)@PES. PES membrane is characterized by an elongated pore structure and a condensed layer at the top of the membrane. The addition of fillers results in a coarser membrane structure on the surface, accompanied by the potential for accumulation due to the uneven distribution of particles. The addition of 30%, MIL-53(Al) was clearly visible on the membrane surface, but the filler particles were more evenly distributed within the PES pores. This filler addition has been demonstrated to facilitate enhanced gas separation capability associated to the PES membrane, a consequence of both the porous and dense layers and the pores changes [47]. Further analysis will be proven through gas permeability testing. The results of this morphological analysis indicate that the addition of MIL-53(Al) at higher loadings (more than 30% w/w) is not recommended as this might induce agglomeration and macroscopic cracks on the membrane. In the membrane for gas separation, channels such as a finger are vital because they provide free hollow space for gas transport to reduce the diffusion paths [48].

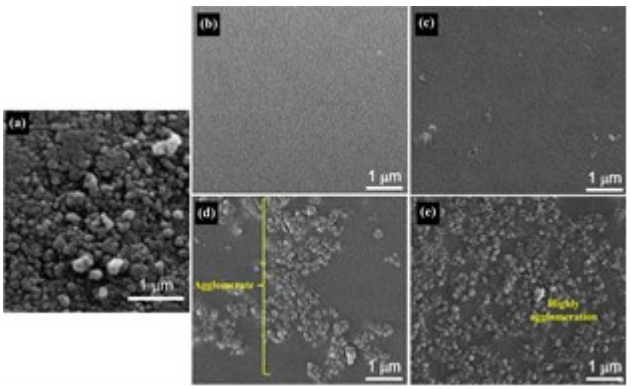


Fig. 5. Surface-section of (a) MIL-53(Al), (b) PES, (c) 10% MIL-53(Al)@PES, (d) 20% MIL-53(Al)@PES, and (e) 30% MIL-53(Al)@PES

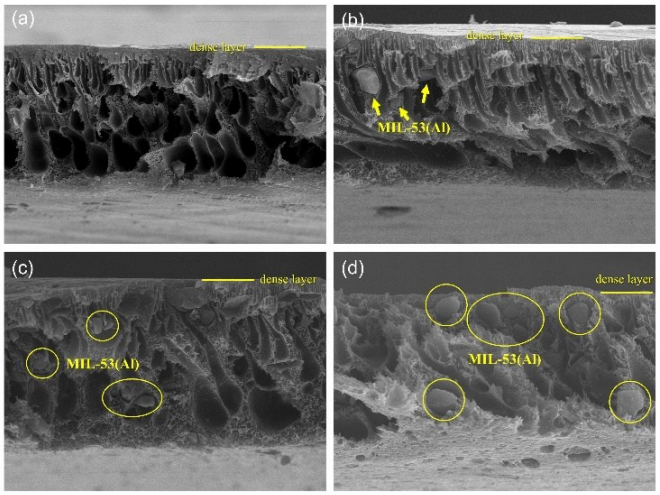


Fig. 6. Cross-section of (a) PES, (b) 10% MIL-53(Al)@PES, (c) 20% MIL-53(Al)@PES, and (c) 30% MIL-53(Al)@PES

### *3.3. Hydrogen separation performance*

The performance of gas separation was determined by conducting a gas permeation test and calculating its absorptivity and selectivity. The measurement of permeability was conducted in $H_2$, $CO_2$, and $CH_4$ single gas systems. The incorporation of higher levels of MIL-53(Al) into the PES resulted in an increase in the selective thickness of the membrane, as evidenced by Fig. 7(a) and Table S4. The addition of the filler results in the disruption of the PES chains and the increase in the void volume of the membranes. This, in tun, results in more uninhibited spots, which facilitates the movement of gases across the PES chains [41]. The selective thickness of the membrane resulted in varied gas permeability values, with the resulting trend being an increase in $H_2$ gas permeability at a thicker selective membrane due to a bigger permeance multiplier (conversion from GPU into Barrer unit). This finding indicates that the selective layer affects the gas solution-diffusion mechanism [49]. The thickest selective layer, measured at 7.628 ± 0.339 µm, is achieved through the addition of 30% MIL-53(Al) on PES, thereby yielding the maximum $H_2$ penetrability.

As illustrated in Fig. 7(b), the selectivity trend for single gas measurement of $H_2$, $CO_2$, and $CH_4$ exhibits the highest selectivity at the addition of 20% MIL-53(Al) on PES. The selectivity of $H_2/CO_2$ and $H_2/CH_4$ values of the PES membrane was measured at 2.12, which enhanced to 3.28 after the addition of 20% MIL-53(Al). The selectivity of $H_2/CO_2$ and $H_2/CH_4$ is equal due to the size of the $H_2$ molecule being much slighter than the size of the $CO_2$ and $CH_4$ molecules. This means that the membrane can more easily allow $H_2$ gas to pass through it than $CO_2$ and $CH_4$ gases which have the potential to cause plasticization. The presence of $CH_4$ in a stiff polymer such as PES has been shown to hamper the diffusion routes for smaller interactive molecules including $H_2$ and $CO_2$ [37]. As a result, the permeability of both gases decreased. In relation to the declining trend of $CO_2/CH_4$ at higher MIL-53(Al) loadings, the presence of $CH_4$ has been shown to reduce the solubility coefficient of $CO_2$, resulting in a decrease in $CO_2$ permeability, as found in many prior investigations [37,50,51,52,53].

The results of single gas ($H_2$, $CO_2$, and $CH_4$) permeability measurements are related to former studies listed in Table 1. The $H_2$, $CO_2$, and $CH_4$ permeability values of PES were determined to be 34.41, 16.15, and 14.93 barrer, respectively. The increased addition of MIL-53(Al) linearly enhanced these gas permeability values attributable to the significant separation mechanism from the flexible MOF filler and its affinity for the related gas molecules.

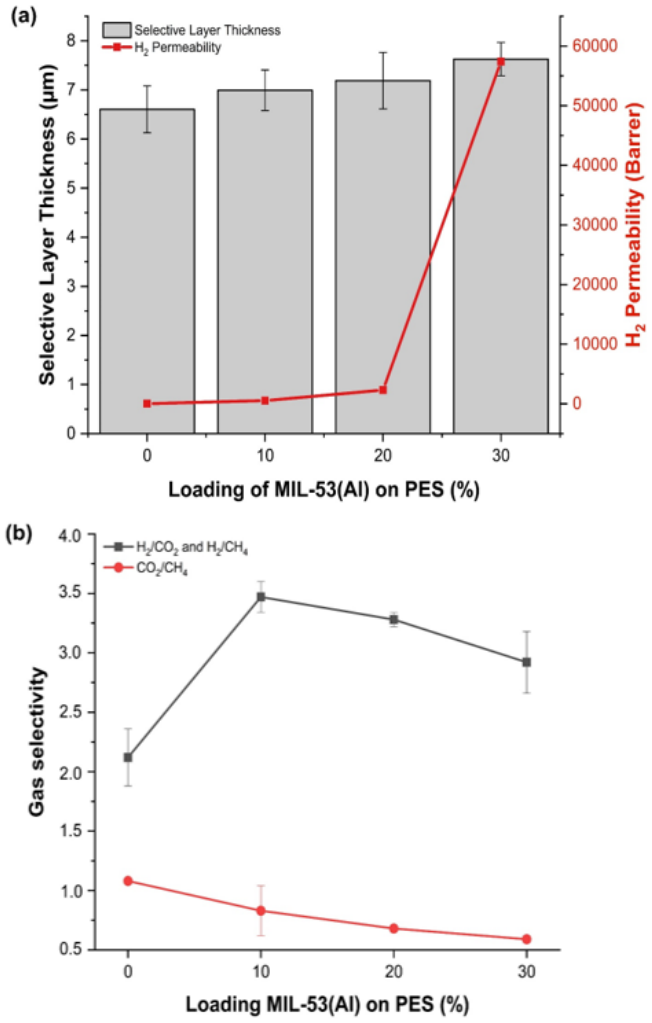


Fig. 7. (a) $H_2$ permeability trend on selective layer thickness is affected by different loading of MIL-53(Al) on PES and (b) Gas selectivity trend of MMMs in single gas measurement

The data position on the Robeson curve indicates the membrane separation performance. As depicted in Fig. 8(a), all membranes examined exhibited superior performance in terms of the Robeson upper bound 2008 for $H_2/CO_2$ gas separation, except for pure PES membrane. This result indicates that MIL-53(Al) fillers improve both permeability and selectivity above the polymer membrane limitation [58]. As illustrated in Fig. 8(b), the membrane that can surpass the line is 30% MIL-53(Al)@PES; however, the 20% MIL-53(Al)@PES approached the Robeson upper bound 1991 for $H_2/CH_4$. Finally, based on the results, it is possible to infer that the performance of MIL-53(Al)@PES met the requirement and appeared to be comparable to other membranes in $H_2$ separation, owing to incredibly high values of $H_2$ permeability, which is highly suitable for industrial processes.

Table 1. Comparison of permeability measurement from MMMs studied in this work with previous research

| Membrane | P (bar) | Permeability (Barrer) | | | Ref. |
|---|---|---|---|---|---|
| | | $H_2$ | $CO_2$ | $CH_4$ | |
| 23% UiO-66-$NH_2$-PVP-PEI | - | 413.76 | 96.00 | - | [54] |
| COC/HKUST-1 40% | 1 | 19.42 | 0.57 | - | [27] |
| COC/MIL-53(Al) 40% | | 16.68 | 0.53 | | |
| CA/C-MOF-5 12% | 6 | 14.95 | 8.41 | - | [55] |
| CA/T-MOF-5 12% | | 13.90 | 7.77 | | |
| VTEC | 5 | 5.00 | 1.00 | - | [56] |
| VTEC/$NH_2$-MIL-53 20% | | 5.40 | 1.00 | | |
| 10% $NH_2$-MIL-53@PI | 3 | 175.00 | 137.00 | 5.00 | [57] |
| PES | 2 | 34.41 | 16.15 | 14.93 | This work |
| 10% MIL-53(Al)@PES | | 547.59 | 189.16 | 228.67 | |
| 20% MIL-53(Al)@PES | | 2307.63 | 702.79 | 1034.96 | |
| 30% MIL-53(Al)@PES | | 57391.61 | 19634.66 | 33336.07 | |

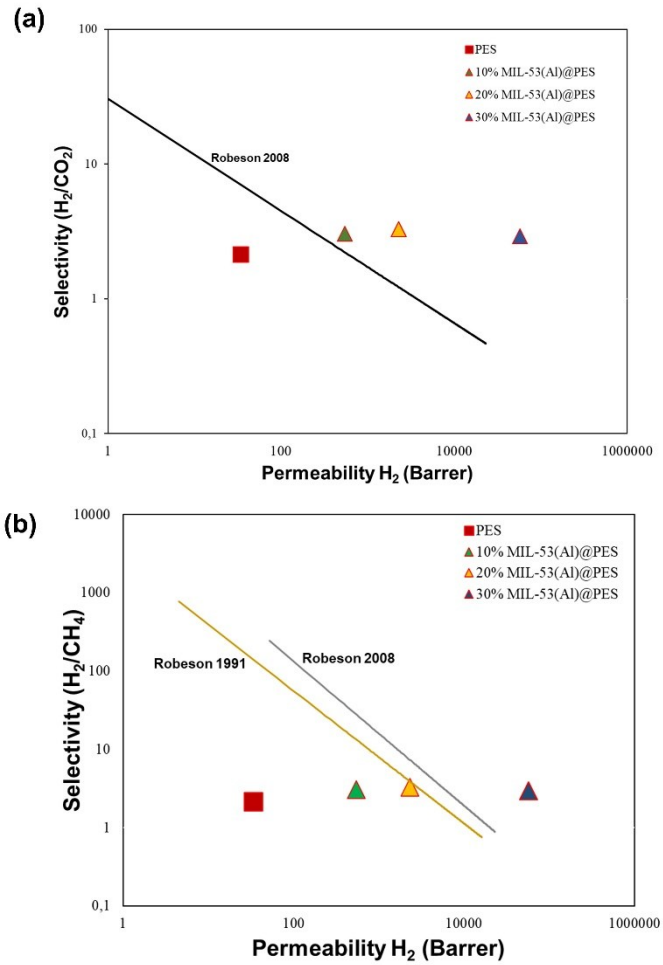


Fig. 8. Robeson curve of MMMs studied in this work [59]

Furthermore, a comparison was made of the performance of PES membrane with that of MMMs 20% MIL-53(Al)@PES was carried out for the mixed gas test. The performance of mixed gas separation was examined using a mixture of $H_2$ and $CH_4$ gas. The results obtained are presented in Table 2. As can be observed, the addition of MIL-53(Al) resulted in a far greater increase in gas permeability of $H_2$, $CO_2$, and $CH_4$. The permeability of $H_2$ gas increased from 21.56 to 1075.93 barrer upon the addition of 20% MIL-53(Al), but the selectivity remained constant. However, the decrease in permeability and selectivity values appears to be quite significant in comparison to the permeability and selectivity of a single gas test. This is possible because of the competitive sorption between the two gases utilized, the polarization of different concentrations, the plasticization of the polymer, and the non-ideal gas phase [37]. Research by Gunawan et al. [37] demonstrated that the permeability of $H_2$ from the $H_2/CH_4$ binary gas test in MMMs P84/ZTC 1 is 36.61 barrer. The results presented in Table 2 demonstrated that 20% MIL-53(Al) exhibited a value exceeding this value.

Table 2. The permeability and selectivity of mixed gas $H_2$-$CH_4$ measurement.

| Membrane | Permeability (Barrer) | | Selectivity |
|---|---|---|---|
| | $H_2$ | $CH_4$ | $H_2/CH_4$ |
| PES | 21.56 ± 3.54 | 11.41 ± 1.87 | 1.89 ± 0.01 |
| 20% MIL-53(Al)@PES | 1075.93 ± 7.65 | 591.00 ± 4.20 | 1.82 ± 0.03 |

## 4. Conclusions

The present study investigates the impact of MIL-53(Al) incorporation into PES on the performance of $H_2$ gas separation. The higher loading of filler MIL-53(Al) has been demonstrated to lead to increased agglomeration, membrane thickness, and gas permeability. The loading MIL-53(Al) into PES, resulted in an outstanding permeability value of 57391.61 barrer by MMMs. Meanwhile, a 20% filler concentration enhanced $H_2/CO_2$ and $H_2/CH_4$ selectivity by 54.72%. These MMMs demonstrate considerable potential for hydrogen production and water-gas shift applications due to their enhanced separation performance.

## Acknowledgements

We would like to express our gratitude to the Ministry of Higher Education, Research, and Technology of the Republic of Indonesia for providing financial support under the project World Class Research (WCR) grant (Project No. 221.1/UN27.22/HK.07.00/2021) and to Universitas Sebelas Maret for funding via the Mandatory Research Grant (Project No. 228/UN27.22/PT.01.03/2023) and Hibah PKGR Project number 462/UN27.22/PT.01.03/2026.

## References

1. T. Zhou, D. Yang, Y. Wang, J. Cheng, Q. Chen, B. Liu, et al., *Low-pressure-RF plasma modification of UiO-66 and its application in methylene blue adsorption,* Plasma Sci. Technol. 25 (2023).

2. H. Asselt, and K. Kulovesi, *Seizing the opportunity: tackling fossil fuel subsidies under the UNFCCC,* Int. Environ Agreements Polit. Law Econ. 17 (2017) 357–370.
3. K. A. Dahl, J. T. Abatzoglou, C. A. Phillips, J. P. Ortiz-Partida, R. Licker, R., L. D. Merner, et al., *Quantifying the contribution of major carbon producers to increases in vapor pressure deficit and burned area in western US and southwestern Canadian forests,* Environ. Res. Lett. 18 (2023).
4. A. El-Ouahrani, J. M. Mesa, and A. Merzouki, A*nthropogenic CO2 emissions from fossil fuels Trends and drivers in the Mediterranean region,* Int. J. Clim. Chang. Strateg. Manag. 3 (2011) 16–28.
5. R. Holze, *On efficiencies, emissions, and the colors of hydrogen—An update,* Energy Storage Convers. 1 (2023) 304–304.
6. K. Oka, Y. Kaiwa, M. Kataoka, K. Fujita, Ichi, and K. Oyaizu, *A Polymer Sheet-Based Hydrogen Carrier*, European J. Org. Chem. (2020) 5876–5879.
7. H. Wang, J. Xu, L. Sheng, X. Liu, Y. Lu, and W. Li, *A review on bio-hydrogen production technology,* Int. J. Energy Res. 42 (2018) 3442–3453.
8. N. Ain, A. M. Amin, H. Fatimah, and M. Zaid, *A Review of Photocatalytic Water Splitting for Hydrogen Production Using Tandem Solar Cell.* (2023).
9. I. Staffell, D. Scamman, A. Velazquez Abad, P. Balcombe, P. E. Dodds, P. Ekins, et al., T*he role of hydrogen and fuel cells in the global energy system,* Energy Environ. Sci. 12 (2019) 463–491.
10. C. J. Quarton and S. Samsatli, T*he value of hydrogen and carbon capture, storage and utilisation in decarbonising energy: Insights from integrated value chain optimisation,* Appl. Energy. 257 (2020).
11. M. S. Akhtar, R. Dickson, and J. J. Liu, L*ife Cycle Assessment of Inland Green Hydrogen Supply Chain Networks with Current Challenges and Future Prospect,.* ACS Sustain. Chem. Eng. 9 (2021) 17152–17163.
12. M. Markiewicz, Y. Q. Zhang, A. Bösmann, N. Brückner, J. Thöming, P. Wasserscheid, et al., *Environmental and health impact assessment of Liquid Organic Hydrogen Carrier (LOHC) systems – challenges and preliminary results,* Energy Environ. Sci. 8 (2015) 1035–1045.
13. A. Golmakani, S. A. Nabavi, and V. Manović, *Effect of impurities on ultra-pure hydrogen production by pressure vacuum swing adsorption,* J. Ind. Eng. Chem. 82 (2020) 278–289.
14. M. El-Shafie, *Hydrogen separation using palladium-based membranes: Assessment of H2 separation in a catalytic plasma membrane reactor,* Int. J. Energy Res. 46 (2022) 3572–3587.
15. S. Nayebossadri, J. D. Speight, and D. Book, *Hydrogen separation from blended natural gas and hydrogen by Pd-based membranes,* Int. J. Hydrogen Energy. 44 (2019) 29092–29099.
16. D. S. G. Subraveti, P. Z. Li, P.V. Prasad, and P.A. Rajendran, *Physics-based neural networks for simulation and synthesis of cyclic adsorption processes,* Industrial & Engineering Chemistry Research. (2022).
17. A.M. Alghamdi, F. Fadhillah, *Thin film composite polyelectrolyte multilayer nanofiltration membrane fabricatedusing spin assisted layer by layer assembly: Application of solution diffusion film mode,* Communications in Science and Technology, 5 (2020) 10–15.
18. B. Haider, M. R. Dilshad, M. Atiq ur Rehman, M. S. Akram, and M. Kaspereit, *Highly permeable innovative PDMS coated polyethersulfone membranes embedded with activated carbon for gas separation,* J. Nat. Gas Sci. Eng. 81 (2020).
19. F. Ahmadijokani, S. Ahmadipouya, H. Molavi, and M. Arjmand, *Amino-silane-grafted NH2-MIL-53(Al)/polyethersulfone mixed matrix membranes for CO2/CH4 separation,* Dalt. Trans. 48 (2019) 13555–13566.
20. P. Gozali-Balkanloo, M. Mahmoudian and, M. T. Hosseinzadeh, *A comparative study between MMT-Fe3O4/PES, MMT-HBE/PES, and MMT-acid activated/PES mixed matrix membranes,* Chem. Eng. J. 396 (2020) 125188.
21. T. D. Kusworo, D.P. Qudratun, Utomo, Indriyanti, and I. R. Ramadhan, *Enhancement of separation performance of nano hybrid PES –TiO2 membrane using three combination effects of ultraviolet irradiation, ethanol-acetone immersion, and thermal annealing process for CO2 remova,* J. Environ. Chem. Eng. 6 (2018) 2865–2873.
22. M. Safak-Boroglu and A. B. Yumru, *Gas separation performance of 6FDA-DAM-ZIF-11 mixed-matrix membranes for H2/CH4 and CO2/CH4 separation,* Sep. Purif. Technol. 173 (2017) 269–279.
23. C. M. Gao, J. C. Chen, S. H. Liu, Y. Q. Xing, S. F. Ji, H. Y. Chen, et al., *Development of hydrophilic PES membranes using F127 and HKUST-1 based on the RTIPS method: Mitigate the permeability-selectivity trade-off,* Environ. Res. 196, (2021).
24. W. W. Lestari, M. A. Khafidhin, R. Wijiyanti, N. Widiastuti, D. S. Handayani, U. S. F. Arrozi, et al, *Novel mixed matrix membranes based on polyethersulfone and MIL-96 (Al) for CO2 gas separation*. Chem. Pap. 75 (2021) 3337–3351 (2021).
25. W. W. Lestari, R. Al Adawiyah, M. A. Khafidhin, R. Wijiyanti, N. Widiastuti, and D. S. Handayani, *CO2gas separation using mixed matrix membranes based on polyethersulfone/MIL-100(Al),* Open Chem. 19, (2021) 307–321.
26. S. C. Hess, R. N. Grass, and W. J. Stark, *MOF Channels within Porous Polymer Film: Flexible, Self-Supporting ZIF-8 Poly(ether sulfone) Composite Membrane,* Chem. Mater. 28 (2016) 7638–7644.
27. N. Ercan, C. Kocyigit, A. Durmus, and A. Kasgoz, *Cyclic olefin copolymer (COC)-metal organic framework (MOF) mixed matrix membranes (MMMs) for H2/CO2 separation,* J. Nat. Gas Sci. Eng. 95, (2021).
28. S. Meshkat, S. Kaliaguine, and D. Rodrigue, *Mixed matrix membranes based on amine and non-amine MIL-53(Al) in Pebax® MH-1657 for CO2 separation.* Sep. Purif. Technol. 200 (2018) 177–190.
29. M. Loloei, S. Kaliaguine, and D. Rodrigue, M*ixed matrix membranes based on NH2-MIL-53 (Al) and 6FDA-ODA polyimide for CO2 separation: Effect of the processing route on improving MOF-polymer interfacial interaction,* Sep. Purif. Technol. 270, (2021).
30. W. W. Lestari, L. Yunita, T. E. Saraswati, E. Heraldy, M. A. Khafidhin, Y. K. Krisnandi, et al., *Fabrication of composite materials MIL-100(Fe)/Indonesian activated natural zeolite as enhanced CO2 capture material,* Chem. Pap. 2021 757. 75 (2021) 3253–3263.
31. S. Basu, A. Cano-Odena, and I. F. J. Vankelecom, *MOF-containing mixed-matrix membranes for CO2/CH4 and CO2/N2 binary gas mixture separations,* Sep. Purif. Technol. 81 (2011) 31–40.
32. R. Adams, C. Carson, J. Ward, R. Tannenbaum, and W Koros, *Metal organic framework mixed matrix membranes for gas separations. Microporous Mesoporous Mater,* 131 (2010) 13–20.
33. S. Japip, Y. Xiao, and T. S. Chung, *Particle-Size Effects on Gas Transport Properties of 6FDA-Durene/ZIF-71 Mixed Matrix Membranes,* Ind. Eng. Chem. Res. 55 (2016) 9507–9517.
34. K. Xie, Q. Fu, J. Kim, H. Lu, Y. He, Q Zhao, et al, *Increasing both selectivity and permeability of mixed-matrix membranes: Sealing the external surface of porous MOF nanoparticles,* J. Memb. Sci. 535 (2017) 350–356.
35. T. Gunawan, R. P. Rahayu, R. Wijiyanti, W. N. W. Salleh, and N. Widiastuti, *P84/Zeolite-Carbon Composite Mixed Matrix Membrane for CO 2 /CH 4 Separation. Indones,* J. Chem. 19 (2019) 650–659.
36. R. Lin, L. Ge, S. Liu, V. Rudolph, and Z. Zhu, *Mixed-Matrix Membranes with Metal–Organic Framework-Decorated CNT Fillers for Efficient CO2 Separation,* ACS Appl. Mater. Interfaces. 7 (2015) 14750–14757.
37. T. Gunawan, N. Widiastuti, H. Fansuri, W. N. Wan Salleh, A F. Ismail, R. Lin, et. al., T*he utilization of micro-mesoporous carbon-based filler in the*

*P84 hollow fibre membrane for gas separation,* R. Soc. Open Sci. 8, (2021).

38. A. Chakraborty and H. Acharya, *Magnetically separable Fe3O4 NPs/MIL-53(Al) nanocomposite catalyst for intrinsic OPD oxidation and colorimetric hydrogen peroxide detection. Colloids Surfaces A Physicochem,* Eng. Asp. 624, (2021).
39. T. R. Katugampalage, C. Ratanatawanate, P. Opaprakasit, C. Kaewsaneha, and P. Sreearunothai, *A smart magnetically separable MIL-53(Al) MOF-coated nano-adsorbent for antibiotic pollutant removal with rapid and non-contact inductive heat regeneration,* Chem. Eng. J. Adv. 8 (2021) 100160.
40. A. Khodayari and S. Sohrabnezhad, *Fabrication of MIL-53(Al)/Ag/AgCl plasmonic nanocomposite: An improved metal organic framework based photocatalyst for degradation of some organic pollutants,* J. Solid State Chem. 297 (2021).
41. J. Han, W. Lee, J. M. Choi, R. Patel, and B. R. Min, *Characterization of polyethersulfone/polyimide blend membranes prepared by a dry/wet phase inversion: Precipitation kinetics, morphology and gas separation.* J. Memb, Sci. 351 (2010) 141–148.
42. T. H. Novita, W. W. Lestari, J. H. Pratama, T. Gunawan, N. Widiastuti, and D. S. Handayani, *Novel mixed matrix membranes (MMMs) based on metal–organic framework (MOF) [Mg3(BTC)2]/poly-ether sulfone (PES): preparation and application for $CO_2$ gas separation*, Journal of Polymer Research, 28 (2021) 434
43. N. Ahadi, S. Askari, A. Fouladitajar, and I. Akbari, *Facile synthesis of hierarchically structured MIL-53(Al) with superior properties using an environmentally-friendly ultrasonic method for separating lead ions from aqueous solutions*, Sci. Rep., 12 (2022) 2649.
44. W. W. Lestari, B. F. Rahman, J. H. Pratama, D. S. Handayani, T. Gunawan, N. Widiastuti, et al., *Fabrication of hybrid membranes based on poly(ether-sulfone)/Materials Institute Lavoisier (MIL-53)(Al) and its enhanced CO2 gas separation performance*, Chemical Papers, 53 (2021) 0123456789.
45. A. Junaidi, U. Zulfiani, A. Khomariyah, T. Gunawan, N. Widiastuti, N. Sazali, et al., *Utilization of polyphenylene sulfide as an organic additive to enhance gas separation performancein polysulfone membranes*, RSC Adv., 14 (2024) 2311–2319.
46. L. Zhu*, H. Yu, H. Zhang, J. Shen, L. Xue, C. Gao, et al., Mixed matrix membranes containing MIL-53(Al) for potential application in organic solvent nanofiltration*, RSC Adv., 5 (2015) 73068–73076
47. S. Yousef, S. Tuckute, A. Tonkonogovas, A. Stankevičius, and A. Mohamed, *Ultra-permeable CNTs/PES membranes with a very low CNTs content and high H2/N2 and CH4/N2 selectivity for clean energy extraction applications,* J. Mater. Res Technol. 15 (2021) 5114–5127.
48. P. Li, R. L. Thankamony, X. Li, Z., Li, X. Liu, and Z. Lai, *Nanoporous polyethersulfone membranes prepared by mixed solvent phase separation method for protein separation,* J. Memb. Sci. 635 (2021).
49. R. W. Baker and B. T. Low, *Gas separation membrane materials: A perspective,* Macromolecules. 47 (2014) 6999–7013.
50. A. Jamil, P. C. Oh, and A. M. Shariff, *Polyetherimide-montmorillonite mixed matrix hollow fibre membranes: Effect of inorganic/organic montmorillonite on CO2/CH4 separation*, Sep. Purif. Technol. 206 (2018), 256–267.
51. R. Ebadi, H. Maghsoudi, and A. A. Babaluo, *Fabrication and characterization of Pebax-1657 mixed matrix membrane loaded with Si-CHA zeolite for CO2 separation from CH4,* J. Nat. Gas Sci. Eng. 90, (2021).
52. M. Z. Ahmad, V. Martin-Gil, T. Supinkova, P. Lambert, R. Castro-Muñoz, P. Hrabanek, et al., *Novel MMM using CO2 selective SSZ-16 and high-performance 6FDA-polyimide for CO2/CH4 separation,* Sep. Purif. Technol. 254, (2021).
53. A. A. Ebadi, M. Omidkhah, and A. Kargari, T*he effects of aminosilane grafting on NaY zeolite-Matrimid®5218 mixed matrix membranes for CO2/CH4 separation,* J. Memb. Sci. 490 (2015) 364–379.
54. S. Ashtiani, M. Khoshnamvand, D. Bouša, J. Šturala, Z. Sofer, A. Shaliutina-Kolešová, et al., *Surface and interface engineering in CO2-philic based UiO-66-NH2-PEI mixed matrix membranes via covalently bridging PVP for effective hydrogen purification,* Int. J. Hydrogen Energy. 46 (2021) 5449–5458.
55. M. Arjmandi, M. Pakizeh, M. Saghi, and A. Arjmandi, *Study of Separation Behavior of Activated and Non-Activated MOF-5 as Filler on MOF-based Mixed-Matrix Membranes in H2/CO2 Separatio,*. Pet. Chem. 584 (2018) 317–329.
56. E. V. Perez, G. J. D. Kalaw, J. P. Ferraris, K. J. Balkus, and I. H. Musselman, *Amine-functionalized (Al) MIL-53/VTEC$^{TM}$ mixed-matrix membranes for H2/CO2 mixture separations at high pressure and high temperature,* J. Memb. Sci. 530 (2017) 201–212.
57. B. Seoane, C. Téllez, J. Coronas, and C. Staudt, *NH2-MIL-53(Al) and NH2-MIL-101(Al) in sulfur-containing copolyimide mixed matrix membranes for gas separation,* Sep. Purif. Technol. 111 (2013) 72–81.
58. Y. Zhao, D. Zhao, C. Kong, F. Zhou, T. Jiang, and L. Chen, *Design of thin and tubular MOFs-polymer mixed matrix membranes for highly selective separation of H2 and CO2,* Sep. Purif. Technol. 220 (2019) 197–205.
59. L. M. Robeson, *Correlation of separation factor versus permeability for polymeric membranes* J. Memb. Sci. 62 (1991) 165–185.